PAPER • OPEN ACCESS

ELM buffering in the MAST Upgrade Super-X divertor

View the article online for updates and enhancements.

ELM buffering in the MAST Upgrade Super-X divertor

Jack Flanagan[1,2,*] ⓘ, **Rory Scannell**[1], **James Bradley**[2] ⓘ, **James Harrison**[1] ⓘ,
Stuart Henderson[1] ⓘ, **Zhouji Huang**[1] ⓘ, **Lucy Kogan**[1] ⓘ, **Nicola Lonigro**[1,3] ⓘ,
Rashed Sarwar[1], **Kevin Verhaegh**[4] ⓘ, **the MAST Upgrade Team**[a]
and the EUROfusion Tokamak Exploitation Team[b]

[1] UKAEA (United Kingdom Atomic Energy Authority), Culham Campus, Abingdon, Oxfordshire OX14 3DB, United Kingdom of Great Britain and Northern Ireland
[2] University of Liverpool, Liverpool L69 7ZX, United Kingdom of Great Britain and Northern Ireland
[3] York Plasma Institute, University of York, York YO10 5DD, United Kingdom of Great Britain and Northern Ireland
[4] Eindhoven University of Technology, Eindhoven, Netherlands

E-mail: jack.flanagan@ukaea.uk

CrossMark

Abstract

The MAST Upgrade Super-X divertor is typically seen to detach in steady state discharges. However, divertor re-attachment is observed to occur during fast transient heat loads. In this paper the effect of edge localised modes (ELMs) on the divertor are diagnosed on fast time scales with Thomson scattering and with a new ultrafast divertor spectroscopy (UFDS) diagnostic. The Thomson scattering data show full ionisation of the detached neutral buffer during large ELM events ($>$2–3 kJ) in a $\sim$1 ms time window after ELMs. Plasma temperature at the strikepoint varies depending on the ELM size and timing reaching up to 10 eV, which is significantly higher than inter-ELM levels but much lower than the pedestal temperatures of $\sim$200 eV. The UFDS diagnostic allows determination of ELM induced reattachment (burn-through) by monitoring the spatial distribution of D_2 Fulcher emission across the divertor. In this initial investigation the ELM energy and divertor neutral gas pressure (P_{gas}) are hypothesised to be the most influential parameters on whether an ELM causes burn-through or not without extrinsic impurities. The relationship of these parameters to burn-through as measured by UFDS is examined by a database of ELMs from MAST-U pulses. For the MAST-U Super-X divertor, the required P_{gas} (in Pa) to buffer an ELM of energy ΔW_{ELM} (in kJ) is estimated to follow a limit of $P_{\mathrm{gas}} \geqslant 0.67\Delta W_{\mathrm{ELM}}$ by a simple model, which is shown to agree well with the experimental results.

---

[a] See Harrison *et al* 2024 (https://doi.org/10.1088/1741-4326/ad6011) for the MAST Upgrade Team.
[b] See Joffrin *et al* 2024 (https://doi.org/10.1088/1741-4326/ad2be4) for the EUROfusion Tokamak Exploitation Team.
[*] Author to whom any correspondence should be addressed.

(Some figures may appear in colour only in the online journal)

1. Introduction

For future tokamaks it is required that plasma facing components can withstand the exhaust from the core confined plasma. The plasma exhaust consists of a steady state power flux into the scrape off layer from the core (P_{SOL}) as well as short transient bursts whose power can greatly exceed steady state P_{SOL}. The requirement to protect plasma facing components is partly fulfilled by detachment [1], the formation of a layer of neutral gas between the plasma facing components of the divertor, or target, and the ionised plasma. Increasing the particle flux into the scrape off layer from the main plasma will typically increase the neutral gas pressure at the target and improve the ability of the detachment front to buffer the plasma exhaust. This has been shown to work well on MAST Upgrade [2] in particular due to the Super-X divertor which greatly improves the ability to maintain a high neutral pressure in the divertor and increases the volume for dissipation of exhaust power before the strike point [2, 3].

Transient events can burn through the neutral gas layer of the detached divertor. This presents a critical risk for future Tokamaks that should be researched on existing machines to ensure the risk is suitably mitigated. These transients can take many forms; edge localised modes (ELMs), sawteeth and H-mode to L-mode back transitions are typical examples but transients can also happen during internal reconnection events (IREs) or even during pellet injection. The allowable transient peak heat flux for tungsten tiles on ITER is $300\,\mathrm{MW\,m^{-2}}$ [4]. This corresponds to $300\,\mathrm{kJ\,m^{-2}}$ of energy flux for typical 1 ms ELM durations, which could be expected from an ELM with energy of 3–6 MJ on ITER, $<1\%$ of the stored plasma energy. For future devices ELMs must be avoided or suppressed for machine survivability [5, 6]. However, not all transients can be avoided, in particular H-L back transitions must occur. This present work utilises ELMs as a convenient transient heat flux to study, but the results and conclusions are relatively general for any transient event releasing an energy ΔW in a timescale t. A study of the effect of detachment on transient heat pulses on Magnum-PSI is presented in [7], the work shows good dissipation or buffering of ELM like events with high detachment.

On MAST upgrade, a typical H-mode inter-ELM P_{SOL} is ~ 1 MW [8], with much of the ohmic heating power and neutral beam power being radiated. As an estimate for the impact of transients on P_{SOL}, small ELMs and large ELMs on MAST-U release 1% and 5% of the 100 kJ of stored plasma energy respectively over a $t_{ELM} \sim 1$ ms, which would result in a transient increase in P_{SOL} to 2 MW and 6 MW respectively. A typical 5 kJ ELM with reasonable estimates of the ELM wetted area in Super-X configuration gives rise to unmitigated energy fluxes of $2.3\,\mathrm{kJ\,m^{-2}}$ or power fluxes of $2.3\,\mathrm{MW\,m^{-2}}$. This is somewhat lower than the corresponding ELM power loads observed on MAST of 10–$20\,\mathrm{MW\,m^{-2}}$ due to the smaller wetted area (radius and width) in MAST [9], which did not have a Super-X divertor.

In this work the effects of the transient P_{SOL} increase due to ELMs on the detached Super-X divertor are investigated with data from divertor Thomson scattering (DTS) [10] and ultrafast divertor spectroscopy (UFDS). By comparing the variation of the D_2 Fulcher emission along the strike leg the UFDS data provides an indicator of the ELM burn-through to the target.

The fraction of the transient energy released into the scrape off layer which is lost before reaching the target, or *buffered fraction*, is a key value to measure. In ASDEX Upgrade [6] the buffered fraction is shown to vary with impurity species which can radiate the transient energy causing it to dissipate more readily than with pure hydrogenic species. For the investigation in this paper, the buffered energy fraction cannot be directly estimated as the infra-red (IR) cameras operated in MAST-U during the third experimental campaign sampled the data every 2.5 ms, which is insufficient to resolve ELMs. Hence this particular element is left for a future work. While the IR data provide a valuable direct measurement of buffered fraction, the UFDS data provides time resolved data within the ELM which are beyond the capabilities of IR. Ultrafast spectroscopy data from the divertor volume also uniquely provides the potential to study the mechanisms of transient power dissipation in more detail.

Section 2 describes the key diagnostics utilised in this work. Section 3 presents divertor Thomson scattering observations of steady state detachment for comparison with observations during transient events in subsequent sections. Section 4 shows individual experimental observations of burn-through from UFDS and DTS. Moving from individual observations to draw more general conclusions, section 5 introduces a database of ELMs compiled to study key parameters and how they relate to burn-through. From this dataset, we are able to predict if an ELM will be buffered or burn through the MAST-U Super-X divertor based on the ELM energy and neutral pressure in the divertor. Section 6 introduces a simple model to demonstrate the expected link between divertor neutral pressure and buffering.

2. Diagnostics

A new diagnostic, UFDS, operates based on avalanche photodiode detectors (APDs) and has been installed in the MAST-U Super-X divertor. It detects D_α, D_β and D_2 Fulcher emission, the latter being captured by a 600 nm central wavelength
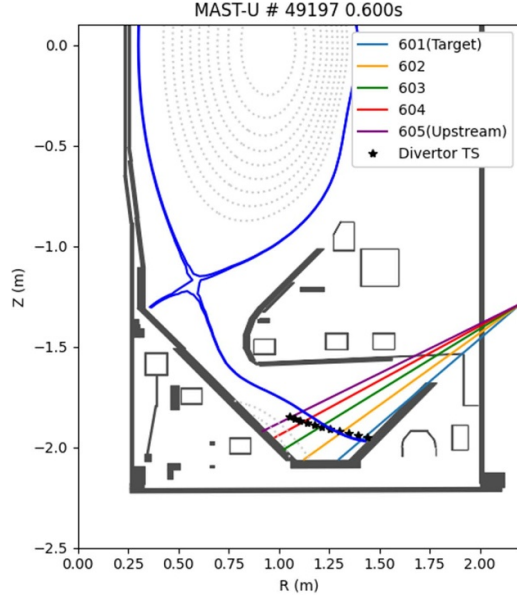
Figure 1. MAST-U geometry showing the last closed flux surface for a typical Super-X divertor pulse examined in this paper with the UFDS lines of sight and DTS scattering centres overlaid.

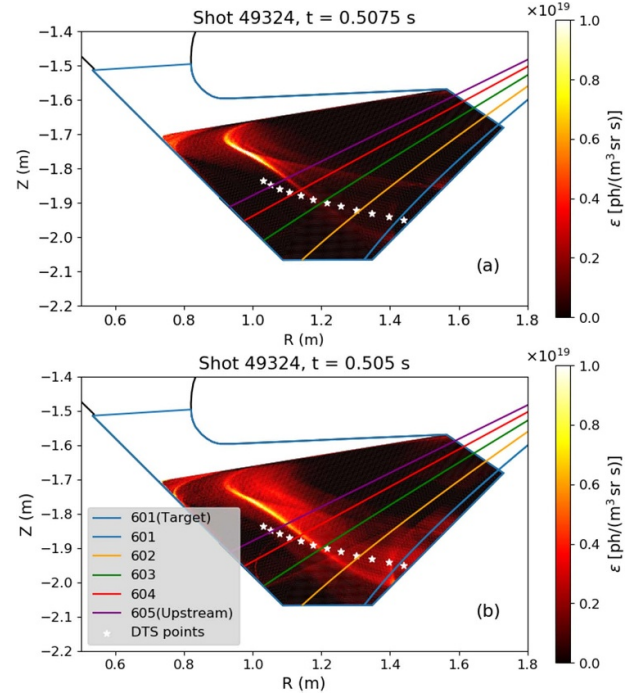**Figure 2.** D_2 Fulcher emission measured by the MWI diagnostic for (*a*) a steady state detached discharge and (*b*) a frame which integrates over an ELM. Lines of sight of UFDS diagnostic and DTS scattering centres are overlaid.

10 nm bandwidth filter. A region of increased D_2 Fulcher emission in the divertor can be used as a proxy for the detachment front which occurs where the plasma and neutral gas dominated regions meet [3]. The APDs were chosen to give very fast response so that ELM and filament dynamics could be observed. The diagnostic was operated with a sampling rate of $800\,\text{kS}\,\text{s}^{-1}$ and bandwidth of $\sim100\,\text{kHz}$ for the data used in this paper. This is sufficient to resolve ELM filament timescales which are typically of order $10\,\mu\text{s}$ [11, 12]. The diagnostic was operated with five lines of sight covering the last $\sim0.5\,\text{m}$ (in the poloidal plane) of the Super-X strike leg in the lower outer divertor as shown in figure 1.

It uses the same collection optics as the divertor Thomson scattering diagnostic [13] and so images fibre bundles on $\sim1\,\text{cm}$ scattering lengths along the strike leg. For the pulses examined, the strike leg is along the focus of the collection optics, as shown in figure 1. Although the UFDS is a line integrated measurement, the observed emission will predominantly come from localised regions along the strike leg which are the overlap of the diagnostic view and strike leg. The measurement positions of the DTS diagnostic [10, 14] which is designed to measure along a chord corresponding to the Super-X strike leg on the outer most tile are also shown in figure 1. The DTS diagnostic measures electron temperature and density in the divertor at each of these measurement positions.

There are existing spectroscopy diagnostics on MAST-U [15] which measure spectral emission along similar lines of sight as the new UFDS diagnostic. These diagnostics are based on grating spectrometers and typically operate at a time resolution of $\sim10\,\text{ms}$. This time resolution is sufficient to resolve steady state situations, but is not capable of resolving transients.

To understand the measurements from the UFDS data it is useful to consider the 2D images obtained from the multi-wavelength imaging diagnostic (MWI) [16]. Figure 2 shows two images of the spatial distribution of D_2 Fulcher emission in the divertor. Figure 2(*a*) shows the D_2 Fulcher emission in a steady state inter-ELM period. During the inter-ELM period the more intense D_2 Fulcher emission does not reach the target, this indicates the divertor leg is detached. The image in figure 2(*b*) is integrated over an ELM and shows the extension of the intense D_2 Fulcher emission up to the target which is indicative of reattachment. It can be seen that during an ELM the emission originates from a broader region than between ELMs. This is not seen to vary significantly between ELMs, and can be assumed to be toroidally symmetric integrated over an ELM discharge. The lines of sight of the UFDS diagnostic are overlaid. Two particular sight lines that we will use frequently in our analysis in this paper are the 'Upstream' view (605—purple) and the 'Target' view (601—blue).

3. Detachment in steady state

To set a baseline for the observations during transients in subsequent sections of this paper, the divertor electron temperature ($T_{\text{e,div}}$) and density ($n_{\text{e,div}}$) profiles in quiescent steady state conditions are examined in figure 3 for three comparable $600\,\text{kA}$ ohmic pulses with on axis toroidal magnetic field $B_{\text{T}} = 0.6\,\text{T}$ and line integral densities varying from $N_{\text{e}} = 0.4$ to $1.2 \times 10^{20}\,\text{m}^{-2}$. These discharges are in Super-X
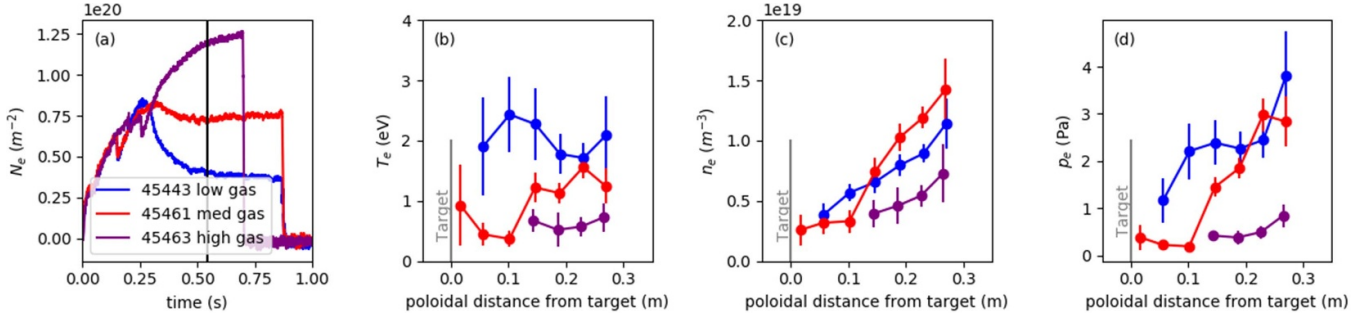
Figure 3. (*a*) Main chamber line integral electron density for three pulses with varying fuelling rates. The laser timing is indicated by the vertical black line. (*b*)–(*d*) Divertor TS electron temperature, density and pressure profiles along the Super-X strike leg.

divertor configuration. While for each shot the main chamber high field side gas fuelling location was used, different voltage waveforms were applied to the piezo gas valve, resulting in the different plasma densities achieved. The plasmas remain in L-mode but would readily transition to H-mode if a beam were applied. The different gas fuelling levels cause a corresponding change in the main chamber line integral electron density (N_e) as shown in figure 3(*a*). The plots figures 3(*b*)–(*d*) show Thomson scattering profiles for the three pulses, the timing of all profiles for all three pulses is at $t = 0.545$ s. All three pulses had similar shaping and the strike legs are very well aligned to the divertor Thomson diagnostic. The electron pressure p_e is calculated by $p_e = n_e k_B T_e$.

The low core density pulse, 45443, has the hottest electron temperature in the divertor with $T_{e,div} \sim 2$ eV right across the divertor Thomson measurement chord. Despite being the lowest core density, it is in the middle in terms of $n_{e,div}$. Relative to the low core density pulse the moderate core density pulse, 45461, has a higher $n_{e,div}$ and lower $T_{e,div}$. The electron pressure in the divertor is approximately conserved comparing the low core density and moderate core density pulses.

Going from the moderate core density pulse to the high core density pulse, 45463, further reduces $T_{e,div}$. However, the high core density pulse has the lowest divertor density. This is caused by the fact that the plasma has gone from detachment, in 45461, to deeper detachment in 45463. DTS data is then unavailable close to the target, as the DTS system cannot measure accurately below a threshold of $T_e \lesssim 0.5$ eV. As it goes into deeper detachment there is an increasingly large neutral fraction in the divertor due to volumetric plasma recombination. Further increasing the main chamber gas rate and density serves to further increase the neutral density in the divertor which in turn increases neutralization of the plasma in the divertor and lowers $n_{e,div}$. Viewed in terms of electron pressure in the divertor, the highest core density pulse has significantly lower pressure than the other two pulses due to this detachment process. These observations from DTS are supported by observations from other diagnostics in these and similar discharges, in particular those of the MWI system observing D_2 Fulcher band emission [3, 16] and visible light spectroscopy.

## 4. Observations of ELM burn-through

4.1. ELM burn-through overview

ELM buffering is the process by which energy released by an ELM into the scrape off layer and the divertor is dissipated before it can reach the target. The dissipation of energy is thought to occur primarily due to hydrogenic and impurity radiation and neutral particle ionisation. Charge exchange may also contribute significantly to the dissipation of ELM energy, and poloidal flux expansion may play an important role in reducing the ELM energy density arriving at the divertor target tiles. Neutral particle recycling could also generate more neutrals to dissipate energy via radiation, molecular dissociation and ionisation, if sufficient recycling can occur within the ELM time scale. Other energy dissipation channels may exist, and the purpose of this research and ongoing simulation work is to understand these processes such that transient buffering may be optimised in future.

We define ELM burn-through as cases in detached divertor scenarios in which the ELM energy is insufficiently buffered and the plasma reattaches to the divertor target tiles. There is no single definition of the boundary between detachment and attachment, however, in this work we consider that the plasma is attached if the ionisation region is attached to the divertor target, which in our data corresponds to a plasma temperature >1 eV at the target.

4.2. DTS measurements of burn-through

Elevated temperatures in the divertor are observed in DTS measurements where profiles are obtained by lasers firing after the transient events. Typical results are shown for three time points obtained in MAST-U pulse 47143 in figure 4. This pulse was an H-mode scenario with 3.1 MW of NBI heating and a double-null Super-X divertor configuration with a line integral density $N_e = \sim 2 \times 10^{-20}$ m^{-2} and a stored plasma energy of 100 kJ. Two time points are obtained within 1 ms of the peak of mid-plane D_α associated with a type I ELM, which are representative of the elevated temperature due to the transient event during the re-attachment. The final time point is 1.5 ms after the ELM and is representative of quiescent profiles of
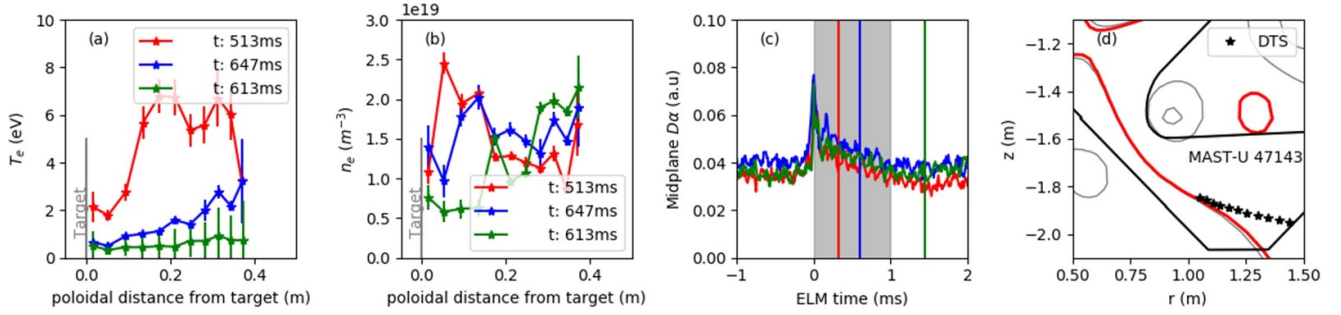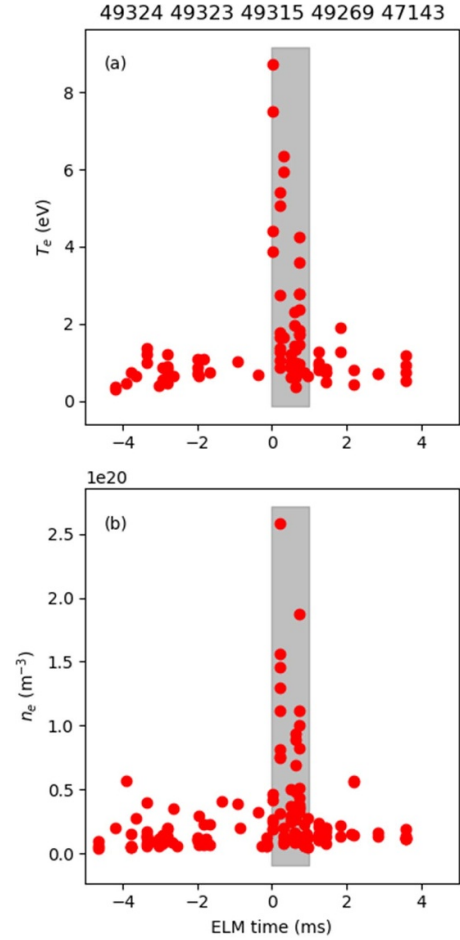
Figure 4. Divertor Thomson scattering profiles for three ELMs in pulse 47143 with (*a*) electron temperature (*b*) electron density and (*c*) timing of the profiles relative the D-alpha peak for each ELM event. (*d*) Shows the alignment of the reconstructed separatrix with the DTS measurement points.

the inter ELM period. For comparison the D_α traces from the three ELMs are super-imposed and shifted to the peak of the mid-plane D_α which we use to calculate the ELM time.

The elevated temperatures of $T_{e,div} \simeq 6\,eV$ during re-attachment are significantly above the inter-ELM values of $\lesssim 1\,eV$, but are much smaller than the upstream pedestal temperature which is in the range of $150 \pm 17\,eV$ where the ELMs are formed. The time-slice closest to the ELM has the highest divertor temperature, but the three spatial points closest to the target show reduced temperature. This may indicate buffering of the transient by the detachment front before the full ELM energy can reach the target. The reduced temperature closer to the target may also be due to the worsening of the DTS alignment with the separatrix closer to the strike point in this case, as can be seen in figure 4(*d*). The divertor neutral pressure during these three ELMs was between 0.24 and 0.33 Pa which is quite low pressure relative to typical MAST-U Super-X conditions in the pulses studied in this paper. These ELMs caused a drop in the line integral core electron density (ΔN_e) of ∼1.9%–2.7% measured by an interferometer, and a drop in the stored plasma energy (ΔW_{ELM}) of 1.1–2.6 kJ as calculated by EFIT [17]. The temperature pedestal and ΔN_e indicate these are small type I ELMs, so we can predict that larger ELMs will readily lead to burn-through. For the particular case shown there is an increase in plasma density close to the target for the time-slices that are taken during the ELM event. From other DTS profiles during ELMs, it is observed that the $n_{e,div}$ and $T_{e,div}$ vary with the neutral gas pressure.

Figure 5 shows divertor Thomson scattering measurements taken from 5 MAST-U pulses with a total of 55 measurement time slices within a 5 ms window of ELM events. These main five pulses are scenarios with a double-null Super-X divertor configuration, stored plasma energies ranging from 80 to 100 kJ, line integrated densities $N_e = 2–2.3 \times 10^{20}\,m^{-2}$, NBI heating powers of 3–3.2 MW, plasma current $I_p = 750\,kA$, and exhibiting both type I and type III ELMs. The full divertor TS data from all spatial points in each time slice are plotted, showing the variation in typical divertor $n_{e,div}$ and $T_{e,div}$ values close to the target at the ELM. As can be seen typical $T_{e,div}$ in the quiescent inter-ELM period are ∼1 eV and values of up to ∼10 eV are seen within 0.5 ms of the ELM event. Typical $n_{e,div}$ in the quiescent inter-ELM period are ∼$1 \times 10^{19}\,m^{-3}$ which can rise up to ∼$20 \times 10^{19}\,m^{-3}$ in the short interval after the

Figure 5. Divertor Thomson scattering measurements across a series of ELMs.

ELM event. The rise in $T_{e,div}$ and $n_{e,div}$ are observed to occur within the 1 ms following the ELM time, this period is shaded in grey in figure 5 and is therefore considered to be a representative timescale for ELM effects in the divertor.

Previous simulation work using the non-linear extended MHD code JOREK [18] predict very high temperatures (>50 eV) in the Super-X going right to the target immediately after the ELM [19]. The qualitative behaviour of the ELM event from measurements presented in this paper is similar,

5
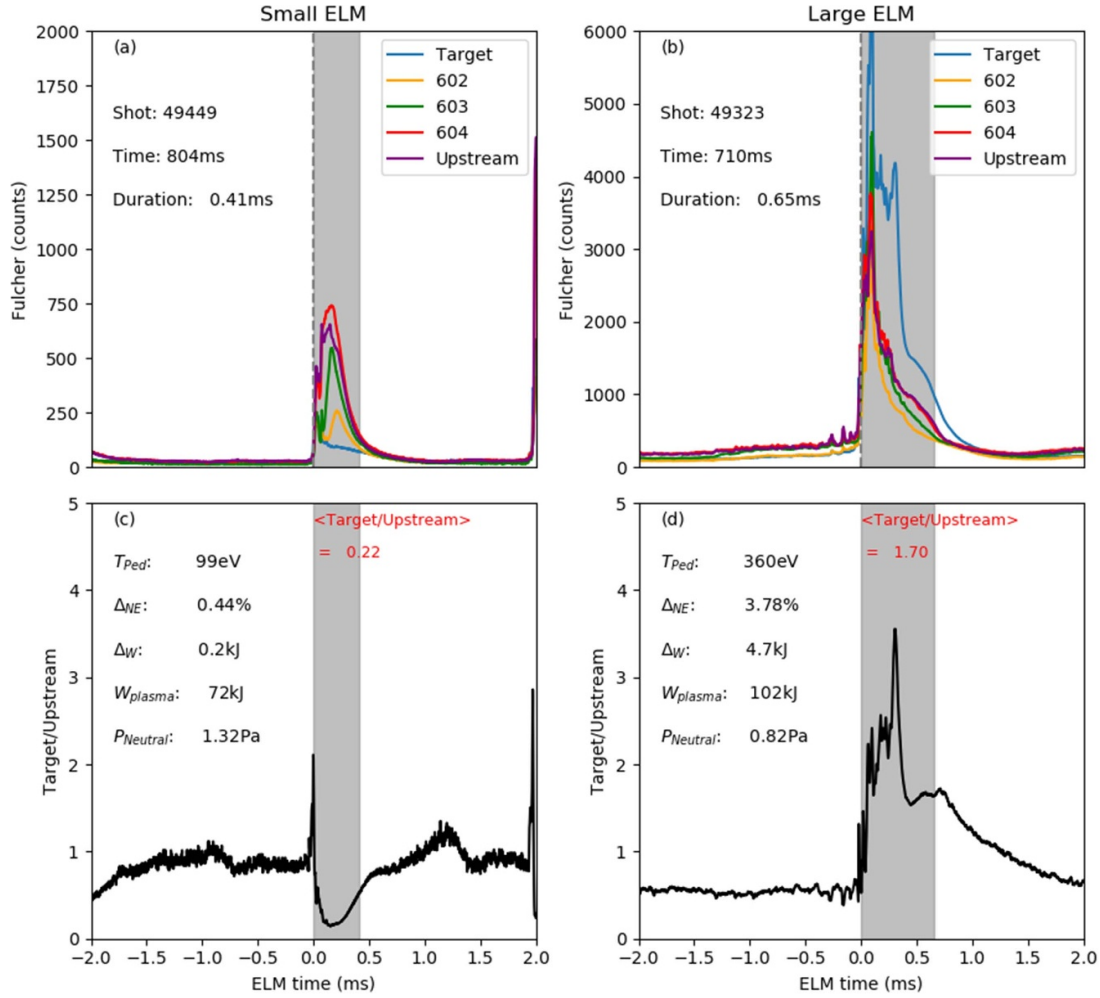
Figure 6. D_2 Fulcher intensities measured by UFDS during (*a*) a small ELM event and (*b*) a large ELM event. The corresponding Target/Upstream ratios are shown for (*c*) the small ELM and (*d*) the large ELM.

but temperatures of this magnitude are not observed. Further JOREK simulations are detailed in [20], again these match well in terms of timescale of the ELM event and electron density observed but predict electron temperatures close to the pedestal temperature in the divertor chamber which have not been replicated in experiment.

4.3. UFDS measurements of burn-through

In contrast to DTS, the UFDS diagnostic operates continuously, capturing every ELM event. Using the edge of the peak of D_2 Fulcher emission as a proxy for the detachment front together with the high temporal resolution of the diagnostic, the location of the detachment front can be resolved during an ELM.

D_2 Fulcher emission can be used in this way due to the conditions in which it is emitted. It is emitted due to the electronic de-excitation of D_2 molecules following electron impact excitation. The threshold energy for such an excitation is around 12 eV, however, at $T_e = 12$ eV D_2 densities are very low as most molecules will have dissociated. Therefore the strongest Fulcher emission occurs in regions of $T_e = 3$–4 eV where a

significant density of D_2 can exist simultaneously with a sufficient number of $\geqslant 12$ eV electrons in the hot tail of the electron Boltzmann distribution [15]. This temperature region coincides with the atomic ionisation region [3], the edge of which can be defined as the detachment front, and therefore the edge of the Fulcher emission region can be taken as a proxy for the detachment front. This proxy is utilised in the rest of this work.

Figure 6(*a*) shows an example of Fulcher band UFDS measurements during a small ELM of $\Delta N_e = 0.44\%$ and $\Delta W_{ELM} = 0.2$ kJ. Over the course of the ELM event, the signal from the channels further upstream increase more than those closer to the target (see figure 2 for the arrangement of the channels). This indicates that the ELM has pushed the ionisation region and detachment front into the view of UFDS. However, the ELM has ultimately been buffered as the intensity of the Fulcher emission reduces significantly before the target. The total duration of this small ELM event observable in the divertor is $\approx$0.41 ms. This is comparable to parallel transport timescales of 0.1–0.3 ms for particles ejected by an ELM travelling from the outboard midplane to the divertor.

Figure 6(*b*) shows the same measurements but for a larger ELM of $\Delta N_e = 3.78\%$, $\Delta W_{ELM} = 4.7$ kJ and duration

≈ 0.65 ms. In this case, besides the Fulcher emission being higher at all points during the ELM, the time evolution is of a different form. The emission rises by a similar magnitude at each spatial point, except for by the target, which increases significantly above the others. This is indicative of burn-through and reattachment, as the front of the Fulcher emission region has fully reconnected to the target. The peak in Fulcher emission at the target may be due to increased ion flux at the target increasing neutral particle recycling which in turn increases molecular deuterium density (if recycling timescales are $\lesssim$ the ELM time scale). The increase in Fulcher emission at the target may also be explained by the increased particle flux causing compression of the neutrals by the target, increasing neutral density and electron density simultaneously, therefore increasing the emission rate. The exact reasons for the high Fulcher emission at the target in these cases requires further research, however, it is taken to be a clear indication of reattachment.

Figures 6(*c*) and (*d*) show the evolution of the ratio of Fulcher emission measured by lines of sight at the target and upstream for the small and large ELM respectively. This Target/Upstream Fulcher ratio is used as a burn-through indicator, where target $<$ upstream, the detachment front is upstream, where target $\sim$ upstream the front has just attached, and where target $>$ upstream, reattachment (burn-through) has occurred. This is clearly illustrated in figure 6: after the small ELM Target/Upstream is $<$1 indicating buffering and after the large ELM $>$ 1 indicating burn-through. To provide a simple numerical indicator for the burn-through status of ELMs the ratio Target/Upstream is averaged for the duration of the ELM event in the following sections of this paper and in figure 6.

UFDS data also provides insight into the timescale of burn-through in the divertor. As seen in figure 6(*a*), the rise in emission occurs later closer to the target. It takes approximately 100 μs for the rise to propagate from the upstream line of sight to that of channel 602, a poloidal distance of $\sim$0.3 m, suggesting a propagation speed of $\sim$3 km s^{-1}. This effect is not seen in the case of the larger ELM of figure 6(*b*), in which the channels all rise within $\sim$20 μs of each other, close to the bandwidth of the diagnostic.

5. ELM burn-through database

5.1. Database overview

To investigate ELM burn-through in different conditions experimentally, a database of $\sim$350 ELMs has been compiled from nine pulses: 49197, 49198, 49200, 49204, 49206, 49312, 49323, 49324 and 49449. All of which are Super-X pulses from the third experimental campaign at MAST-U. These discharges have plasma currents of 750 kA and injected neutral beam heating powers of 1.3–3.3 MW. The resulting plasmas have $q_{95} = 5.97$–6.37, plasma energies of 70–123 kJ and ELM frequencies of 50–600 Hz, pedestal top parameters are as shown in figure 7(*a*). The divertor was in a detached state in all pulses between ELMs, the gas pressure of the neutral cloud varied throughout the pulses from $\sim$0.2–1.4 Pa. This variation is partly due to different upstream densities across

the pulses. Additionally, the neutral pressure in the divertor typically increases throughout a pulse.

For each individual ELM event key parameters are recorded in a database. These parameters include the ELM time t_{ELM}, taken to be at the peak of the mid-plane D_α emission associated with the ELM, τ_{ELM}, the duration of the ELM as measured by the duration of increased D_α emission following the ELM observed by the upstream UFDS channel, and P_{gas}, the neutral gas pressure measured by a fast ion gauge in the divertor at t_{ELM}. Also recorded are ΔN_e, the change in the core line integrated electron density, and ΔW_{ELM}, the change in stored plasma energy as measured by EFIT, both measured across the ELM duration τ_{ELM}, and the Target/Upstream Fulcher ratio referred to in section 4.2 which is averaged across τ_{ELM} to indicate burn-through. ΔN_e is not converted into an average density across the width of the plasma to prioritise the direct measurement. An appendix is included for further explanation and discussion of the measurement procedures involved in the database.

Figure 7 shows the database data for all nine pulses while the strike point radius was > 1.4 m and $P_{gas} < 1.35$ Pa. These filters ensure that the divertor was in Super-X configuration for good UFDS coverage and that the fast ion gauge was not saturated [8]. The colouring of the points for all six plots corresponds to the pedestal electron temperature ($T_{e,ped}$). Figure 7(*a*) illustrates the range of pedestal top parameters in the database. Higher $T_{e,ped}$ leads to lower collisionality which results in larger ELMs. Figure 7(*b*) shows the range of ELM frequency and energy in the dataset. A low energy, high frequency tail is seen, characteristic of type III ELMs. There is also a group of high energy and low frequency ELMs, which are likely to be type I ELMs. Approximately 100 ELMs out of the 350 in the database are estimated to be type I.

Figure 7(*c*) shows the ELM duration distribution with ELM energy, generally with more energetic ELMs causing a longer disturbance. Figure 7(*d*) shows the relationship between ELM energy and ELM particle loss. ELMs causing greater particle loss generally carry more energy, but the relationship is not linear. The non-linearity is partly expected to be due to the different nature of the particle loss mechanism between type I and type III ELMs (convective/conductive) [21, 22]. In addition the energy loss due to an ELM will have a dependence on the pedestal temperature prior to the event [21], introducing further variation to the $\Delta W_{ELM} - \Delta N_e$ relationship.

Figure 7(*e*) shows the variation of burn-through with the ELM energy as measured by EFIT. Larger ΔW ELMs, which may be seen to be correlated to $T_{e,ped}$, are more likely to cause burn-through and burn through more intensely, that is at higher Target/Upstream ratio. Figure 7(*f*) shows variation of the Target/Upstream ratio of the D_2 Fulcher emission or burn-through state with P_{gas}, showing that the transients are more effectively buffered at higher pressure.

The uncertainty in ΔW_{ELM}, $\sigma_{\Delta W}$, is predominantly due to high point to point variation in the stored plasma energy calculated by EFIT. This variation has been measured in the ELM free periods of the shots in the data base, leading to an estimation of $\sigma_{\Delta W} = \pm 0.9$ kJ on average. Additional uncertainty exists in the measurement of shorter duration ELMs due to the
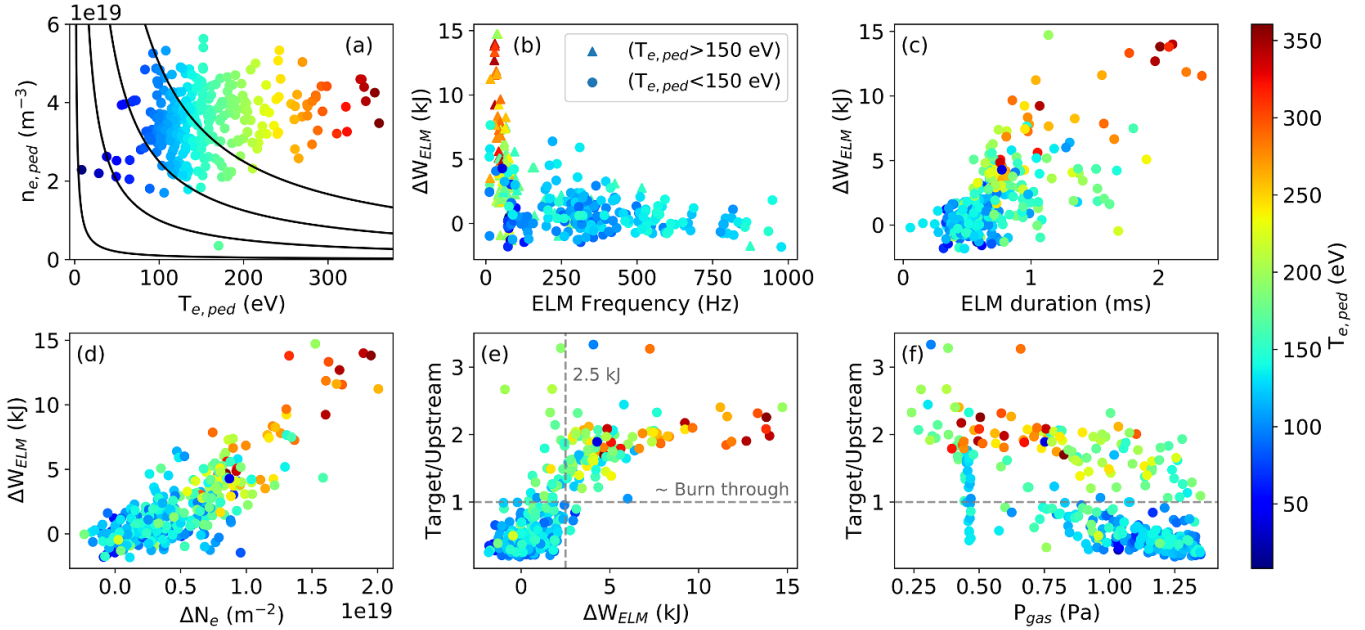
Figure 7. ELMs from nine plasma discharges, where each dot represents an ELM event, showing (*a*) the pedestal temperature and density (*b*) the relationship between ELM energy loss and ELM frequency (*c*) the relationship between ELM energy and duration (*d*) the relationship between the energy loss and line integral density loss over the ELM (*e*) Target/Upstream Fulcher emission versus energy loss over the ELM (*f*) Target/Upstream Fulcher emission versus divertor neutral pressure.

relatively slow 0.6 ms time resolution of the EFIT calculations. The temporal resolution of EFIT is limited by the resolution of magnetic diagnostics. The interferometer used to measure ΔN_e has a time resolution of 20 μs which is much faster than the ELM events. Larger ELMs have longer durations, up to 2.5 ms, as shown by figure 7(*c*), and are well resolved by both measurements.

It can be seen that in general ELMs related to higher ΔW_{ELM} are more likely to cause burn-through, and a lower neutral pressure in the divertor will also make burn-through more likely. This agrees with predictions from [8]. It can also be seen that generally the high $T_{\mathrm{e,ped}}$ ELMs are larger in particle count and energy, and are more likely to cause burn-through. It can be seen in figure 7(*e*) that ELMs greater than 2.5 kJ in energy are likely to cause burn-through the MAST-U Super-X divertor. In MAST type I ELMs were found to occur only at $T_{\mathrm{e,ped}} \gtrsim 150$ eV [23], it can be seen in figure 7(*e*) that ELMs with $T_{\mathrm{e,ped}} \gtrsim 150$ eV make up the majority of those which cause burn-through. This suggests that avoiding type I ELMs by operating in a type II ELMy QCE regime, a candidate considered for both SPARC and STEP [24, 25], may reduce the risk of burn-through. The role of plasma shaping in controlling ELM behaviour is an active area of research [26–28].

5.2. Effects of neutral pressure and ELM energy on burn-through likelihood

As introduced in section 4 the energy dissipation channels enabling ELM buffering are thought to be hydrogenic and impurity radiation, neutral particle ionisation, charge exchange, and possibly neutral particle recycling and poloidal

flux expansion. The exploration of the role of impurity seeding on transient buffering in MAST-U is left for future work, hence all the pulses in the database are unseeded. Hydrogenic radiation and neutral particle ionisation losses will both be proportional to the number of neutral particles in the ELM path. Assuming that most neutral particles will be encountered in the divertor the likelihood of ELM burn-through is therefore expected to be dependant on the divertor neutral gas pressure, P_{gas}, related to the number of particles in the path by the gas temperature and ELM path volume by the ideal gas law.

At this stage measuring the divertor gas temperature and ELM path volume require significant analysis. It is also expected the ELM path volume may not vary significantly, as detached Super-X pulses have reasonably stable detachment front positions between 0.4 and 0.5 m from the target and all pulses in the database had similar levels of poloidal flux expansion. Therefore, in this initial work ELM burn-through as indicated by the UFDS Fulcher ratio is investigated for varying ΔW_{ELM} and P_{gas}, considered likely to be the most influential parameters for ELM buffering.

Figure 8(*a*) shows the ΔW_{ELM} versus P_{gas} measurements for all ELMs from the database with the points coloured by the Target/Upstream ratio, ELMs recorded with a strike point radius < 1.4 m or $P_{\mathrm{gas}} > 1.35$ Pa are excluded as in figure 7. Physically ΔW_{ELM} can only be positive, however it can be measured to be negative for low ΔW ELMs due to the estimated uncertainty $\sigma_{\Delta W}$ shown by the error bars. Taking Target/Upstream >1 and <1 to indicate burn-through and buffering of transients respectively, we can calculate the percentage of ELMs which caused burn-through, displayed in figure 8(*b*). The bins are sized in the ΔW_{ELM} axis by the estimated uncertainty.
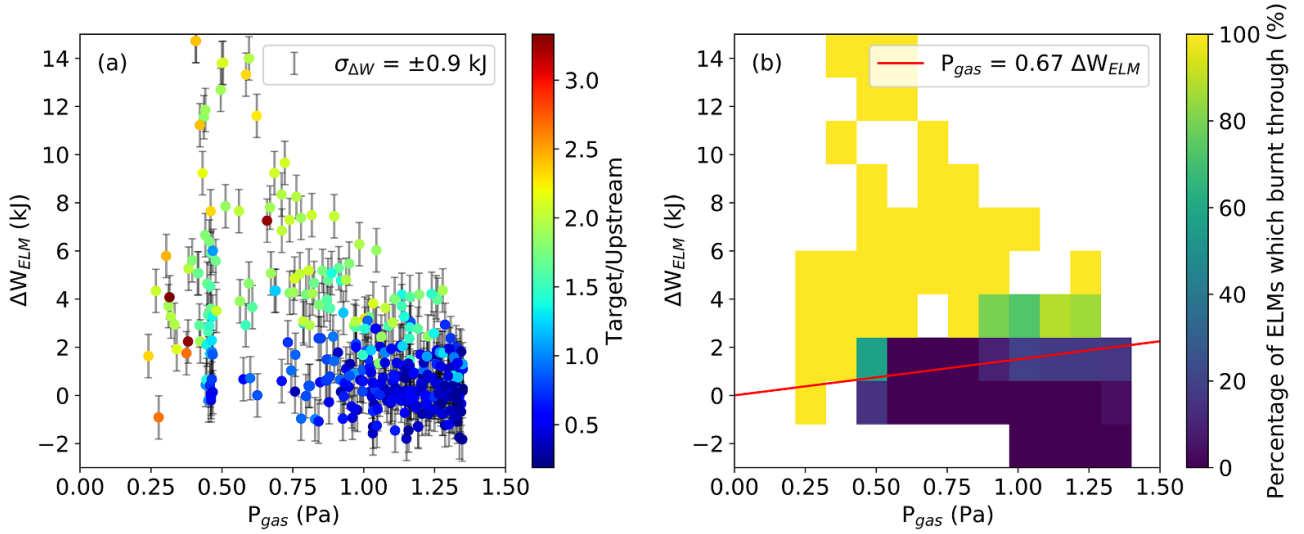
Figure 8. (*a*) Target/Upstream Fulcher emission for all suitable ELMs from 9 Super-X pulses plotted at each ELM ΔW_{ELM} and divertor P_{gas}. (*b*) The data is collected into bins which are coloured corresponding to the percentage of ELMs inferred to have caused burn-through within that bin. Note the number of ELMs in each bin varies, visible by comparison to (*a*). Equation (4) is superimposed on (*b*) for reference.

From figure 8 we can see a clear expected trend of increased probability of burn-through with higher ΔW_{ELM}. Lower P_{gas} also appears to increase the probability of burn-through for a given ΔW_{ELM} as predicted.

6. ELM buffering by ionisation of neutral particles

6.1. Description of model

Here a simple model is introduced based on the mechanics of ELM buffering as introduced in section 4. Energy loss due to ionisation of neutral molecular deuterium is considered. Radiative losses, charge exchange, and neutral particle recycling are as of yet not included. Impurities are also left for future consideration.

Firstly, the total energy released by an ELM, ΔW_{ELM}, will be shared between the inner and outer SOL, and the lower and upper divertor in double-null configuration (standard in MAST-U). As the key diagnostics used for this analysis are in the lower outer divertor we calculate the ELM energy delivered to this divertor as

$$\Delta W_{\mathrm{ELM,out,low}} = \Delta W_{\mathrm{ELM}} f_{\mathrm{out}} f_{\mathrm{low}}, \qquad (1)$$

where f_{out} and f_{low} are the fractions of ELM energy flowing into the outer SOL and lower divertor respectively. The total ionisation energy of the neutral cloud in the path of the ELM per divertor, E_{buffer}, will be proportional to the number of neutral particles in this volume, N_{buffer}, multiplied by the energy required to ionise each particle. N_{buffer} will depend on the volume of the path and the density within that volume. Using the ideal gas law to determine the density of the neutral gas cloud, and assuming the neutral cloud is

made up of solely molecules,

$$E_{\mathrm{buffer}} = A L_{\mathrm{pol}} \left(E_{\mathrm{dissoc}} + 2 E_{\mathrm{ion}} \right) \frac{P_{\mathrm{gas}}}{T_{\mathrm{gas}}}, \qquad (2)$$

where A is the cross sectional area of the path, L_{pol} is the poloidal distance of the detachment front from the target, P_{gas} and T_{gas} are the pressure and temperature of the neutral gas, and E_{dissoc} and E_{ion} are the dissociation energy of a deuterium molecule and ionisation energy of a deuterium atom respectively.

If $\Delta W_{\mathrm{ELM, lower, outer}} \geqslant E_{\mathrm{buffer}}$, or

$$\Delta W_{\mathrm{ELM}} \geqslant \frac{A L_{\mathrm{pol}}}{f_{\mathrm{out}} f_{\mathrm{low}}} \left(E_{\mathrm{dissoc}} + 2 E_{\mathrm{ion}} \right) \frac{P_{\mathrm{gas}}}{T_{\mathrm{gas}}}, \qquad (3)$$

the ELM will cause burn-through. From past IR thermography measurements $f_{\mathrm{out}} = 0.8$ and $f_{\mathrm{low}} = 0.5$ can be estimated for typical connected double-null MAST-U discharges [29, 30]. From MWI measurements of SXD discharges typical L_{pol} values are 0.4 m. A is estimated by the width of ELM induced heat flux in the divertor in the poloidal plane, multiplied by the toroidal circumference of the neutral cloud in the divertor chamber. Assuming the major radius of the centre of the neutral cloud to be ~1.3 m, the toroidal extent is 8.2 m. MWI measurements integrated over ELMs from the database, such as shown in figure 2(*b*), were used to find the average poloidal extent. The cross-field width of ELM induced D_2 Fulcher emission across the neutral cloud in the divertor was measured, finding the average poloidal extent of the ELM path to be 0.15 m, giving $A \approx 1.2 \, \mathrm{m}^2$. Multiplying by L_{pol} yields an approximation of the volume of the ELM path through the neutral detachment cloud to be 0.49 m^3. Ignoring the Franck–Condon model, we estimate $E_{\mathrm{dissoc}} = 4.4 \, \mathrm{eV}$ and $E_{\mathrm{ion}} = 13.6 \, \mathrm{eV}$ [31, 32]. Using

the above, we estimate an ELM of $\sim 1.2\,\text{kJ}$ will cause burn-through at $P_{\text{gas}} = 0.8\,\text{Pa}$. Alternatively, assuming all variables are constant while varying P_{gas}, the neutral pressure required to buffer an ELM is estimated to follow:

$$P_{\text{gas,MAST-U}} \geqslant 0.67 \times \Delta W_{\text{ELM}}. \qquad (4)$$

The prediction of equation (4) is compared to the data collected in this work in figure 8(*b*), which shows reasonable agreement.

6.2. Model discussion

Equation (3) is similar to a model to estimate the time taken for a transient power flux to burn-through a detachment front developed by Henderson *et al*, see equations (6)–(8) in [33]. This model was developed for slow transients and has been validated for transients with durations of $\sim 10\,\text{ms}$ on MAST-U, $\sim 0.1\,\text{s}$ on ASDEX Upgrade and $\sim 1\,\text{s}$ on JET [8]. The model also takes into account deuterium recycling, which is more relevant for slower transients.

Equation (3) could be improved by acknowledging that the neutral cloud is made up of a mixture of atomic and molecular deuterium. The cross sectional area of the ELM path, A, can be used to incorporate poloidal flux expansion into the model. The inequality of equation (3) can be considered to generally include the energy loss mechanisms ignored so far. Gas temperatures in the divertor chamber have been measured up to $\sim 0.5\,\text{eV}$ [15]. However, the fast ion gauge used to measure neutral pressure is located in the sub-divertor, where the room temperature assumption is likely to be valid. If we assume the number density of neutral particles is equal in the divertor and sub-divertor, using room temperature is valid as this is the temperature at which the pressure is measured. The neutral gas pressure in the ELM path through the divertor is assumed to return to equilibrium between ELMs.

Due to the list of assumptions made the comparison of equation (4) to the data shown in figure 8(*b*) is not expected to be predictive, but to validate the basic approach of the model.

7. Conclusions and future work

A new spectroscopy diagnostic has been used in the MAST Upgrade Super-X divertor to determine for individual ELM events whether or not they cause burn-through to the target. For a purely deuterium plasma it has been shown that the probability of ELM burn-through is well predicted by two parameters: divertor neutral pressure and ELM energy loss. The maximum neutral pressure diagnosed thus far in the Super-X divertor is $1.4\,\text{Pa}$, this has been shown to be able to buffer up to $2.5\,\text{kJ}$ of ELM energy, much lower than maximum ELM energies of around $10\,\text{kJ}$. The majority of ELMs measured to have caused burn-through were likely type I ELMs, supporting the avoidance of type I ELMs as intended in next generation tokamaks.

To complement the spectroscopy measurements Thomson scattering has been used to measure T_e and n_e profiles in the Super-X during ELM burn-through. This has shown electron temperatures generally elevated for 1 ms after the ELM and of

up to $\sim 10\,\text{eV}$ within 0.5 ms of the ELM, much higher than the inter-ELM values but lower than pedestal temperatures.

The data from these diagnostics show that although the Super-X divertor allows for excellent steady state detachment, transient events will readily cause burn-through. This re-enforces the requirement that transient events must be prevented or mitigated in a reactor device. Despite this, initial results indicate the neutral buffer facilitated by detachment and the Super-X divertor configuration plays a key role in ELM buffering, which could be leveraged in future tokamaks.

A number of different avenues are envisaged to expand this present analysis, with a view to enhancing understanding and improving buffering:

Pulse configuration: obtain pulses with a Super-X strike leg with a variety of detachment front locations and connection lengths to see if these parameters have a measurable effect on burn-through.

Diagnostic capabilities: high time resolution infrared data will be captured in future campaigns at MAST-U. The IR data will enable direct measurements of ELM energy transferred to the divertor tiles, and therefore quantitative estimates of the buffered ELM energy fraction. The UFDS diagnostic will also be increased from 5 to 10 channels to allow for better spatial resolving of the location of the detachment front.

Transient types: different transients such as H–L back transitions and sawteeth will be added into the analysis of transient burn-through.

Actuators: utilise divertor D_2 puffing to further investigate the effect of D_2 pressure on buffering. Extend analysis to include investigating the effects of impurity seeding on ELM buffering, a key potential solution to protecting divertor tiles in future.
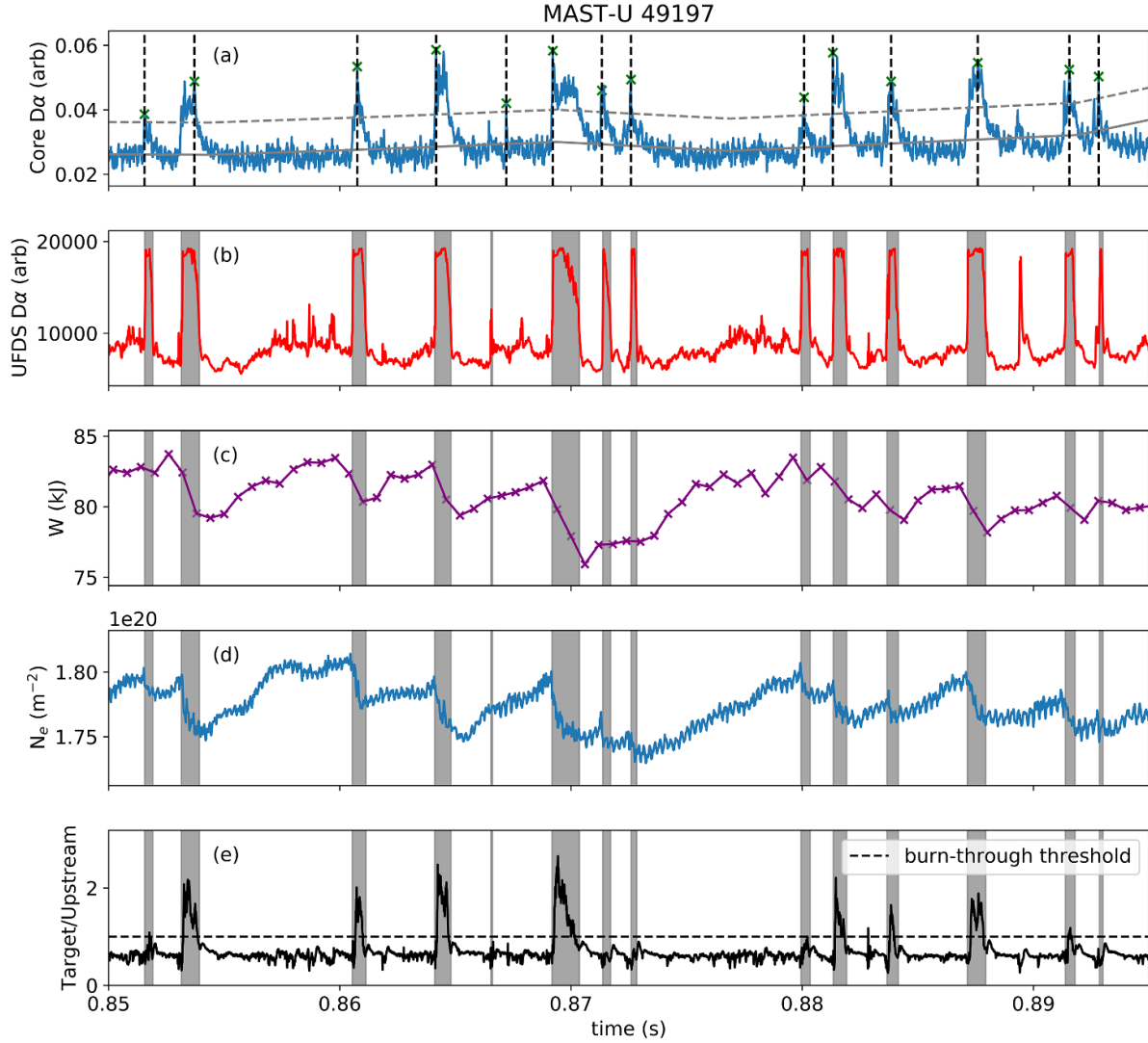
Acknowledgments

Appendix. Database measurement methods

To create the ELM database introduced in section 5, a reliable and accurate system for measuring each parameter relating to the ELMs was required. The measurement procedure is shown

Figure 9. An example of ELM database measurements showing (*a*) ELM identification by core D_α emission and (*b*) subsequent ELM duration estimation using divertor D_α emission. The duration estimation is then used to calculate: (*c*) ΔW_{ELM} by the stored plasma energy estimated by EFIT, (*d*) ΔN_e by the line integrated electron density and (*e*) the Target/Upstream Fulcher ratio using UFDS D_2 Fulcher emission measurements.

by figure 9. First, ELMs are identified by peaks in the core D_α signal measured by a filtered fibrescope. The time correlating to each peak is taken to be the ELM time, t_{ELM}. An alternative definition of the ELM time is by the beginning of the rise in D_α emission. However, as can be seen in figure 9(*a*), the rise time is fast ($<500\,\mu$s) and for use as a basis of further measurements the D_α peak time is sufficient.

The divertor D_α signal as measured by UFDS is then used to identify a start and end time for each ELM, indicated in figures 9(*b*)–(*e*) by the shaded areas. The ELM start and end times are measured by finding the extrema of the edges of the peak in this signal either side of t_{ELM}. These are found by where the signal crosses a fixed low threshold above its inter-ELM background. The ELM start and end times are used to calculate τ_{ELM}. They are also used in the measurement of ΔW_{ELM}, ΔN_e and the Target/Upstream Fulcher ratio which are made across the duration of the ELM.

Due to the similar sampling rate of W as measured by EFIT (0.6 ms) compared to a typical ELM duration (<1 ms) precise

ΔW_{ELM} measurements are challenging, as seen in figure 9(*c*). To measure ΔW_{ELM} the difference is taken between the stored plasma energy measurements preceding the ELM start time and following the ELM end time. The estimation of uncertainty in the ΔW_{ELM} measurement is discussed in section 5.1.

ΔN_e is measured by the difference in the line integral electron density between the ELM start and end times, and Target/Upstream is measured by the average of its value in the period between these times. Other values such as P_{gas} for each ELM are taken by their interpolated value exactly at t_{ELM}. No uncertainty is introduced by this interpolation as these measurements are insensitive to an ELM, and do not vary significantly across one.

ORCID iDs

Jack Flanagan ⬤ 0009-0006-8443-6435
James Bradley ⬤ 0000-0002-8833-0180
James Harrison ⬤ 0000-0003-2906-5097

Stuart Henderson 🔵 0000-0002-8886-1256
Zhouji Huang 🔵 0000-0002-0175-2648
Lucy Kogan 🔵 0009-0002-9158-4920
Nicola Lonigro 🔵 0000-0001-8581-0384
Kevin Verhaegh 🔵 0000-0002-0500-2764

References

[1] Leonard A.W. 2018 Plasma detachment in divertor tokamaks *Plasma Phys. Control. Fusion* **60** 044001

[2] Harrison J.R. *et al* 2024 Overview of physics results from MAST Upgrade towards core-pedestal-exhaust integration *Nucl. Fusion* **64** 112017

[3] Verhaegh K. *et al* (The MAST Upgrade Team) 2022 Spectroscopic investigations of detachment on the MAST Upgrade Super-X divertor *Nucl. Fusion* **63** 016014

[4] Linke J. *et al* 2011 Performance of different tungsten grades under transient thermal loads *Nucl. Fusion* **51** 073017

[5] Eich T., Sieglin B., Thornton A.J., Faitsch M., Kirk A., Herrmann A. and Suttrop W. 2017 ELM divertor peak energy fluence scaling to ITER with data from JET, MAST and ASDEX upgrade *Nucl. Mater. Energy* **12** 84–90

[6] Komm M., Faitsch M., Henderson S., Bernert M., Brida D., Février O., Järvinen A., Silvagni D. and Tskhakaya D. (The ASDEX Upgrade Team and The EUROfusion MST1 Team) 2023 Mitigation of divertor edge localised mode power loading by impurity seeding *Nucl. Fusion* **63** 126018

[7] Federici F., Lipschultz B., Akkermans G.R.A., Verhaegh K., Reinke M.L. and Classen I.G.J. (Magnum-PSI Team) 2024 Effect of detachment on Magnum-PSI ELM-like pulses: direct observations and qualitative results *Nucl. Fusion* **64** 126068

[8] Henderson S.S. *et al* 2024 Validating reduced models for detachment onset and reattachment times on MAST-U *Nucl. Mater. Energy* **41** 101765

[9] Thornton A.J., Allan S.Y., Dudson B.D., Elmore S.D., Fishpool G.M., Harrison J.R. and Kirk A. 2017 The role of ELM filaments in setting the ELM wetted area in MAST and the implications for future devices *Plasma Phys. Control. Fusion* **59** 014047

[10] Clark J.G., Bowden M.D. and Scannell R. 2021 Low temperature Thomson scattering on MAST-U *Rev. Sci. Instrum.* **92** 043545

[11] Scannell R., Kirk A., Ayed N.B., Carolan P.G., Cunningham G., McCone J., Prunty S.L. and Walsh M.J. 2007 Experimental investigation into ELM filament formation on MAST *Plasma Phys. Control. Fusion* **49** 1431

[12] Kirk A. 2008 Comparison of the filament behaviour observed during type I ELMs in ASDEX Upgrade and MAST *J. Phys.: Conf. Ser.* **123** 012012

[13] Hawke J., Scannell R., Harrison J., Huxford R. and Bohm P. 2013 Outline of optical design and viewing geometry for divertor Thomson scattering on MAST Upgrade *J. Instrum.* **8** C11010

[14] Clark J.G., Bowden M.D., Kim Y., Parry B., Rose E., Sarwar R. and Scannell R. 2022 First divertor Thomson scattering measurements on MAST-U *Rev. Sci. Instrum.* **93** 103534

[15] Osborne N., Verhaegh K., Bowden M.D., Wijkamp T., Lonigro N., Ryan P., Pawelec E., Lipschultz B., Soukhanovskii V. and van den Biggelaar T. (The MAST-U Team) 2023 Initial Fulcher band observations from high resolution spectroscopy in the MAST-U divertor *Plasma Phys. Control. Fusion* **66** 025008

[16] Wijkamp T.A. *et al* (The MAST Upgrade Team) 2023 Characterisation of detachment in the MAST-U Super-X divertor using multi-wavelength imaging of 2D atomic and molecular emission processes *Nucl. Fusion* **63** 056003

[17] Kogan L. *et al* 2022 First MAST-U equilibrium reconstructions using the EFIT++ code *48th EPS Conf. on Plasma Physics (Europhysics Conf. Abstracts) (27 June–1 July 2022) (Maastricht, Netherlands)* (European Physical Society (EPS)) (available at: http://ocs.ciemat.es/EPS2022PAP/pdf/P2a.116.pdf)

[18] Hoelzl M. *et al* 2021 The JOREK non-linear extended MHD code and applications to large-scale instabilities and their control in magnetically confined fusion plasmas *Nucl. Fusion* **61** 065001

[19] Harrison J.R. *et al* (The MAST-U Team and The EUROfusion MST1 Team) 2019 Overview of new MAST physics in anticipation of first results from MAST Upgrade *Nucl. Fusion* **59** 112011

[20] Smith S.F., Pamela S.J.P., Fil A., Hölzl M., Huijsmans G.T.A., Kirk A., Moulton D., Myatra O., Thornton A.J. and Wilson H.R. (The JOREK Team) 2020 Simulations of edge localised mode instabilities in MAST-U Super-X tokamak plasmas *Nucl. Fusion* **60** 066021

[21] Kirk A. *et al* (The MAST Team) 2004 ELM characteristics in MAST *Plasma Phys. Control. Fusion* **46** 551

[22] Leonard A.W. 2014 Edge-localized-modes in tokamaks *Phys. Plasmas* **21** 090501

[23] Kirk A., O'Gorman T., Saarelma S., Scannell R. and Wilson H.R. (The MAST Team) 2009 A comparison of H-mode pedestal characteristics in MAST as a function of magnetic configuration and ELM type *Plasma Phys. Control. Fusion* **51** 065016

[24] Eich T. *et al* 2025 The separatrix operational space of next-step fusion experiments: from ASDEX Upgrade data to SPARC scenarios *Nucl. Mater. Energy* **42** 101896

[25] Meyer H. (on the behalf of the STEP Plasma Team) 2024 Plasma burn—mind the gap *Phil. Trans. R. Soc. A.* **382** 20230406

[26] Snyder P.B., Wilson H.R., Ferron J.R., Lao L.L., Leonard A.W., Mossessian D., Murakami M., Osborne T.H., Turnbull A.D. and Xu X.Q. 2004 ELMs and constraints on the H-mode pedestal: peeling–ballooning stability calculation and comparison with experiment *Nucl. Fusion* **44** 320

[27] Holcomb C.T. *et al* 2009 Optimizing stability, transport and divertor operation through plasma shaping for steady-state scenario development in DIII-D *Phys. Plasmas* **16** 056116

[28] Imada K., Osborne T.H., Saarelma S., Clark J.G., Kirk A., Knolker M., Scannell R., Snyder P.B., Vincent C. and Wilson H.R. (The MAST Upgrade Team) 2024 Observation of a new pedestal stability regime in MAST Upgrade H-mode plasmas *Nucl. Fusion* **64** 086002

[29] De Temmerman G., Delchambre E., Dowling J., Kirk A., Lisgo S. and Tamain P. 2010 Thermographic study of heat load asymmetries during MAST L-mode discharges *Plasma Phys. Control. Fusion* **52** 095005

[30] Harrison J.R., Bowman C., Clark J.G., Kirk A., Lovell J., Patel B.S., Ryan P., Scannell R., Thornton A.J. and Verhaegh K. 2024 Benefits of the Super-X divertor configuration for scenario integration on MAST Upgrade *Plasma Phys. Control. Fusion* **66** 065019

[31] Kramida A., Ralchenko Y. and Reader J. (NIST ASD Team) 2024 *NIST Atomic Spectra Database (ver. 5.12)* (National Institute of Standards and Technology) (available at: https://physics.nist.gov/asd) (Accessed 8 September 2025)

[32] Huber K.P. and Herzberg G. 1979 *Constants of Diatomic Molecules* (Springer)

[33] Henderson S.S. *et al* (The ASDEX Upgrade Team and The EUROfusion MST1 Team) 2023 Divertor detachment and reattachment with mixed impurity seeding on ASDEX Upgrade *Nucl. Fusion* **63** 086024